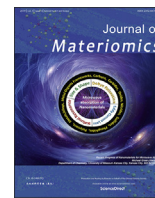




Contents lists available at ScienceDirect

Journal of Materiomics

journal homepage: www.journals.elsevier.com/journal-of-materiomics/

Conventional sintered Cu_{2-x}Se thermoelectric material

Zhiming Geng ^{a,1}, Dongliang Shi ^{a,1}, Lu Shi ^a, Ying Li ^a, G. Jeffrey Snyder ^b, Kwok-ho Lam ^{a,*}

^a Department of Electrical Engineering, The Hong Kong Polytechnic University, Hung Hom, Kowloon, Hong Kong

^b Department of Materials Science and Engineering, Northwestern University, Evanston, USA

ARTICLE INFO

Article history:

Received 8 April 2019

Received in revised form

22 June 2019

Accepted 26 June 2019

Available online 29 June 2019

Keywords:

Thermoelectric

Copper selenide

Copper-vacancy engineering

Effective mass model

ABSTRACT

As the featured material of the superionic thermoelectric (TE) material family, copper-chalcogenide Cu_{2-x}Se is attracting growing research interest for its excellent TE performance derived from the satisfactory power factor and the ultra-low thermal conductivity induced by the superionic effect. Various efforts have been made and proved to be effective to further enhance the TE performance for Cu_{2-x}Se . However, this material is still far from the application stage, which is mainly due to concerns regarding control of the properties and the costly complex fabrication technology. Here we report a scalable pathway to achieve high-performance and tunable Cu_{2-x}Se , utilizing conventional sintering technology and copper (Cu)-vacancy engineering with an effective mass model. The figure of merit zT is a competitive value of 1.0 at 800 K for the optimized binary Cu_{2-x}Se , based on the precise modeling prediction and Cu-vacancy engineering. The changes in TE properties of Cu_{2-x}Se under heating-cooling cycle tests are also revealed. Our work offers the referable method along with the decent parent material for further enhancement of TE performance, paving a possible route for the application and industrialization of Cu_{2-x}Se TE materials. © 2019 The Chinese Ceramic Society. Production and hosting by Elsevier B.V. This is an open access article under the CC BY-NC-ND license (<http://creativecommons.org/licenses/by-nc-nd/4.0/>).

1. Introduction

Calls for new green energy technology have been raised due to ever increasing issue on fossil fuel shortage and environment problems [1–3]. However, statistics revealed that over 60% energy is wasted worldwide mostly as emissions of heat [4,5]. Intrinsically as a cutting-edge energy technology, the solid-state thermoelectric (TE) technology offers a decent solution to solve this energy problem in a simple and environment-friendly way. Serving as the core component for TE technology, the TE materials are capable to harvest and convert waste heat to electricity directly, and the reverse direct pumping of heat with electricity is also realizable [6–10]. Growing attention is thus being paid to TE technology because of the unique feature of TE materials, as well as the advantages over other energy technologies: small size, no moving parts, high reliability and broad temperature-range use [11–17].

The conversion efficiency for a specific TE material is determined mostly by the thermoelectric figure of merit $zT = (S^2\sigma)T/\kappa$, where S , σ , κ and T are thermopower (Seebeck coefficient),

electrical conductivity, total thermal conductivity and absolute temperature, respectively [18,19]. Here $S^2\sigma$ is also defined as the power factor (PF), and the total thermal conductivity κ includes both the contributions from the lattice thermal conductivity κ_L and the electronic thermal conductivity κ_e , which is expressed by $\kappa = \kappa_L + \kappa_e$ [20]. Heavily depending on the figure of merit zT , the performance of TE materials is aimed to be enhanced through two aspects: to improve the electrical properties (S , σ and PF) and to reduce the thermal conductivity. Thus, various means have been utilized to achieve high zT , such as band structure engineering, nanostructuring, etc [21–30]. However, it is still challenging because the electrical and thermal transport in materials are strongly coupled in which the increase of PF may induce the increase of κ , or vice versa [31–35]. Therefore, it turns out to be important to find a TE material with intrinsic superior electrical properties and low thermal conductivity, following the concept of phonon-glass electron-crystal [36,37].

As the featured material of copper chalcogenides Cu_{2-x}X ($\text{X} = \text{S}, \text{Se}$ or Te), Cu_{2-x}Se is of growing TE study interest due to its superionic nature at high temperature. At low temperature below about 400 K, Cu_{2-x}Se presents a low-symmetry monoclinic crystal structure, known as the α -phase. Upon heating above 400 K, a reversible phase transition takes place [38–40], then Cu_{2-x}Se exhibits a superionic cubic structure with the space group $\text{Fm}\bar{3}\text{m}$, which is the β -phase of Cu_{2-x}Se [41,42]. In superionic β - Cu_{2-x}Se , Se^{2-} ions occupy

* Corresponding author.

E-mail address: kokokh.lam@polyu.edu.hk (K.-h. Lam).

Peer review under responsibility of The Chinese Ceramic Society.

¹ Contributed equally.

at the face-centered lattice, while Cu^+ ions can be found at the octahedral 4b sites, tetrahedral 8c sites, and trigonal 32f sites. Cu^+ ions are kinetically free and thus can travel freely among their respective positions within the Se^{2-} framework just like a “liquid” [43–45]. Attributed to this featured superionic nature, the phonon (thermal) transport can be effectively scattered by the diffusion of Cu^+ ions, thus low thermal conductivity is obtained. Also owing to the good electrical properties with tunable capability, Cu_{2-x}Se is now recognized as a promising TE material.

Although the superionic nature of Cu_{2-x}Se favors the TE performance, it also induces reliability concerns. The diffusive Cu^+ ions at high temperature facilitate copper migration in a thermal or electrochemical gradient in Cu_{2-x}Se [46–48], which can be an obstacle to the application of this kind of TE material.

Moreover, there is other stumbling block to be tackled to further the application and realize the industrialization. As generally known, product performance, reliability and cost are the major factors to be considered before mass-production. At present, TE materials are still suffering from high cost, including complex fabrication methods of hot-pressing (HP) and spark plasma sintering (SPS) as solidification technologies, which are actually difficult to be introduced to industry. To tackle this situation, the conventional sintering technology can be considered alternatively, which is much more cost-effective and scalable and has been widely utilized in industry. Therefore, it is of great significance to explore the feasibility of applying conventional sintering technology to the fabrication of Cu_{2-x}Se , to advance its industrialization.

In this work, we report that the TE performance of conventional sintered Cu_{2-x}Se can be precisely optimized via Cu-vacancy engineering using effective mass modeling as a guide [49,50]. An optimized zT value of ~ 1.0 is achieved at 800 K for the undoped Cu_{2-x}Se , and the excellent repeatability in properties is also obtained from room temperature to 800 K. This work offers a readily scalable and cost-effective path to fabricate Cu_{2-x}Se material with high TE performance and good thermal reliability, heading a great step to its industrialization. Besides, this Cu-vacancy engineered Cu_{2-x}Se can be a decent parent TE material for further study focusing on the TE performance enhancement.

2. Experimental

2.1. Sample preparation

Cu_{2-x}Se ($x = 0.03, 0.02$ and 0.01) samples with nominal compositions were synthesized via conventional solid-state sintering technology. Oxygen-free Cu shots (99.99%, Aladdin) and Se shots (99.999%, Aladdin) were used as the raw materials. The stoichiometry-determined Cu and Se shots were weighed and mixed. The whole processing was operated in glove box. The mixture was then sealed in a carbon-coated quartz crucible, melted at 1440 K for 3 h, followed with annealing at 973 K. The as-prepared ingot was ground into fine powder in glove box using an agate mortar, then weighed and pressed into discs under a pressure of 240 MPa. Finally, the discs with a typical diameter of 14 mm and a thickness of 0.5 mm were sintered at 973 K for 2 h under an argon atmosphere, and then naturally cooled down to room temperature.

2.2. Characterizations

The phase structures of the as-sintered bulk samples were determined by X-ray diffraction (XRD) at room temperature with a X-ray diffractometer (Rigaku SmartLab), in which Cu K_α radiation ($\lambda = 1.5406 \text{ \AA}$) was used.

The scanning electron microscopy (SEM) was performed with a scanning electron microscope (Tescan VEGA3) at room

temperature, the bulk samples were cracked to expose the fracture morphology. Owing to the good electrical conductivity of the samples, the coating of gold (Au) was not implemented before conducting SEM.

The electronic transport features including the Seebeck coefficient (S) and the electrical conductivity (σ) as well as the thermal cycling test were performed using a thermal system (Netzsch SBA 458 Nemesis, Germany) adopting the four-probe method, under an argon atmosphere with a flow rate of 50 mL min^{-1} . The thermal conductivity was obtained through the calculation of $\kappa = D \cdot C_p \cdot d$, where the thermal diffusivity (D) was measured using a laser flash analysis instrument (Netzsch LFA 457 MicroFlash, Germany) under an argon atmosphere with a flow rate of 50 mL min^{-1} , a constant specific heat capacity (C_p) [47] was used rather than a decreasing high-temperature heat capacity used in the recent literature [51], and the geometric density (d) was measured.

3. Results and discussions

Fig. 1 shows the room-temperature XRD patterns of the Cu-vacancy engineered Cu_{2-x}Se ($x = 0.03, 0.02$ and 0.01) samples. The XRD patterns exhibit identical characteristics of monoclinic Cu_2Se phase (Standard Identification Card, JCPDS: 27-1131) for the conventional sintered Cu_{2-x}Se samples. With increasing Cu vacancies, the cubic Cu_2Se phase (Standard Identification Card, JCPDS: 06-0680) forms, resulting in the coexistence of monoclinic and cubic phases. This reveals the dependence of the room-temperature phase structure of Cu_{2-x}Se on the Cu-vacancy concentration, and the phase structure could be tuned via Cu-vacancy engineering for Cu_{2-x}Se . The SEM images for the cross-sections of the Cu_{2-x}Se samples are shown in Fig. 2. All samples are confirmed to be well densified after sintering, exhibiting stacked-plate grain structures. The grain sizes are revealed to be micron-level.

The temperature-dependent electronic transport properties, electrical conductivity (σ), Seebeck coefficient (S) and power factor (PF), of the as-fabricated Cu_{2-x}Se samples are plotted in Fig. 3. For all samples, the electrical conductivity decreases with ramping temperature up to 800 K, and undergoes a featured α - β phase transition influence of Cu_{2-x}Se at $\sim 400 \text{ K}$, which is indicated by the abrupt change of electrical conductivity (Fig. 3a). It is also coincident to the expectation that the electrical conductivity diminishes with higher Cu stoichiometry (less Cu vacancies), for instance, the electrical conductivity at room temperature decreases from $\sim 2000 \text{ S cm}^{-1}$ for $\text{Cu}_{1.97}\text{Se}$ to $\sim 750 \text{ S cm}^{-1}$ for $\text{Cu}_{1.99}\text{Se}$. This trend is well attributed to the p-type semiconductor nature of Cu_{2-x}Se in which more Cu

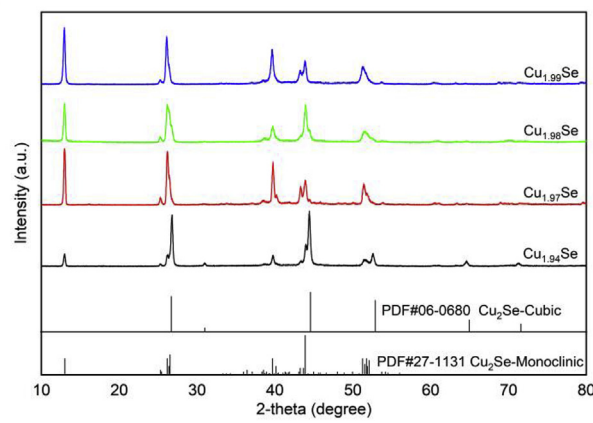


Fig. 1. Room-temperature XRD patterns for the Cu-vacancy engineered Cu_{2-x}Se ($x = 0.03, 0.02$ and 0.01).

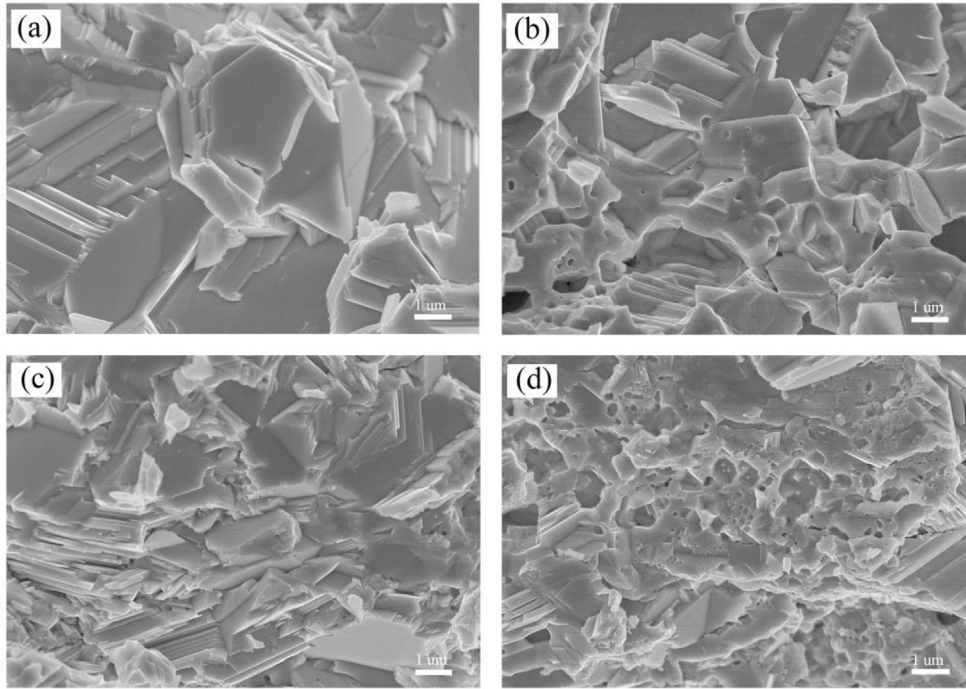


Fig. 2. SEM images for the cross-sections of the as-sintered Cu_{2-x}Se bulk samples. (a) $\text{Cu}_{1.97}\text{Se}$, (b) $\text{Cu}_{1.98}\text{Se}$, and (c) $\text{Cu}_{1.99}\text{Se}$.

vacancies greatly increase the hole concentration and thus facilitate the charge transport. The p-type semiconductor nature is also revealed by the positive values of Seebeck coefficient of Cu_{2-x}Se (Fig. 3b). The trend of Seebeck coefficient is just inverse to that of electrical conductivity, which increases with the temperature and is negatively related to the concentration of Cu vacancies. No evident bipolar effect is observed up to 800 K, and the optimal Seebeck coefficient of $\sim 240 \mu\text{V K}^{-1}$ is obtained for $\text{Cu}_{1.99}\text{Se}$ at 800 K. The power factor ($PF = S^2\sigma$) is calculated based on the measured σ and S , and plotted as a function of temperature (Fig. 3c). All the Cu_{2-x}Se samples show the same trend in the power factor as a function of temperature. For the α -phase Cu_{2-x}Se , the power factors are $6.5\text{--}7.5 \mu\text{W cm}^{-1} \text{K}^{-2}$, and competitive values of $8\text{--}11.5 \mu\text{W cm}^{-1} \text{K}^{-2}$ are obtained for the β -phase at 800 K [51]. Overall, the electronic transport properties are successfully tuned and optimized through Cu-vacancy engineering, and the satisfactory power factors are thus achieved for the Cu_{2-x}Se samples.

Based on the low thermal diffusivity measured for Cu_{2-x}Se (Fig. 4a), the thermal conductivity values of β -phase Cu_{2-x}Se are calculated to be small, as plotted in Fig. 4b. It is evident that samples with less Cu vacancies show lower thermal conductivity over the whole temperature range. The extremely low thermal conductivity is achieved for $\text{Cu}_{1.99}\text{Se}$ at 800 K, which is due to the small amount of Cu vacancies and the superionic nature at high temperature. This is consistent with the expectation based on the electrical conductivity analysis in which lower carrier concentration (indicated by the lower electrical conductivity) contributes less electronic thermal conductivity to the total thermal conductivity, which will be further discussed in the following part.

Ascribing to the optimized power factor and low thermal conductivity, high zT is realized with Cu-vacancy engineering, reaching the maximum value of ~ 1.0 at 800 K for $\text{Cu}_{1.99}\text{Se}$ as shown in Fig. 5. Excellent tunability is revealed that the zT value increases exactly with the decreasing Cu vacancy. Besides, higher zT is expected if the measurement temperature is further elevated, based on the trend

in zT as a function of temperature.

To better understand the thermal transport mechanism for β -phase Cu_{2-x}Se , the samples with nominal compositions ($\text{Cu}_{1.97}\text{Se}$, $\text{Cu}_{1.98}\text{Se}$ and $\text{Cu}_{1.99}\text{Se}$) close to stoichiometric Cu_2Se are evaluated to further study the contribution of carriers (electronic contribution) to the total thermal conductivity. The Lorenz number, L , is defined according to the equation:

$$L = \left(\frac{k_B}{e}\right)^2 \left\{ \frac{\left(r + \frac{7}{2}\right) F_{r+\frac{5}{2}}(\eta)}{\left(r + \frac{3}{2}\right) F_{r+\frac{1}{2}}(\eta)} - \left[\frac{\left(r + \frac{5}{2}\right) F_{r+\frac{3}{2}}(\eta)}{\left(r + \frac{3}{2}\right) F_{r+\frac{1}{2}}(\eta)} \right]^2 \right\} \quad (1)$$

where k_B is the Boltzmann constant, e is the electron charge, $F(\eta)$ is the Fermi-Dirac integral, η is the reduced chemical potential and r represents the carrier scattering factor (acoustic phonon scattering $r = -1/2$ is adopted in the present case [52,53]). Based on the effective mass model, the reduced chemical potential can be obtained from the Seebeck coefficient as a function of temperature, addressing from the equation:

$$S(\eta) = - \left(\frac{k_B}{e}\right) \left[\frac{\left(r + \frac{5}{2}\right) F_{r+\frac{3}{2}}(\eta)}{\left(r + \frac{3}{2}\right) F_{r+\frac{1}{2}}(\eta)} - \eta \right] \quad (2)$$

Then the Lorenz number can be derived, which is a monotone function of the reduced chemical potential. As shown in Fig. 6a, the Lorenz number reduces against temperature, ascribed to the increase of reduced chemical potential that is indicated by the trend of Seebeck coefficient (Fig. 3b). The Lorenz number calculated based on this approach is more precise, compared with the directly

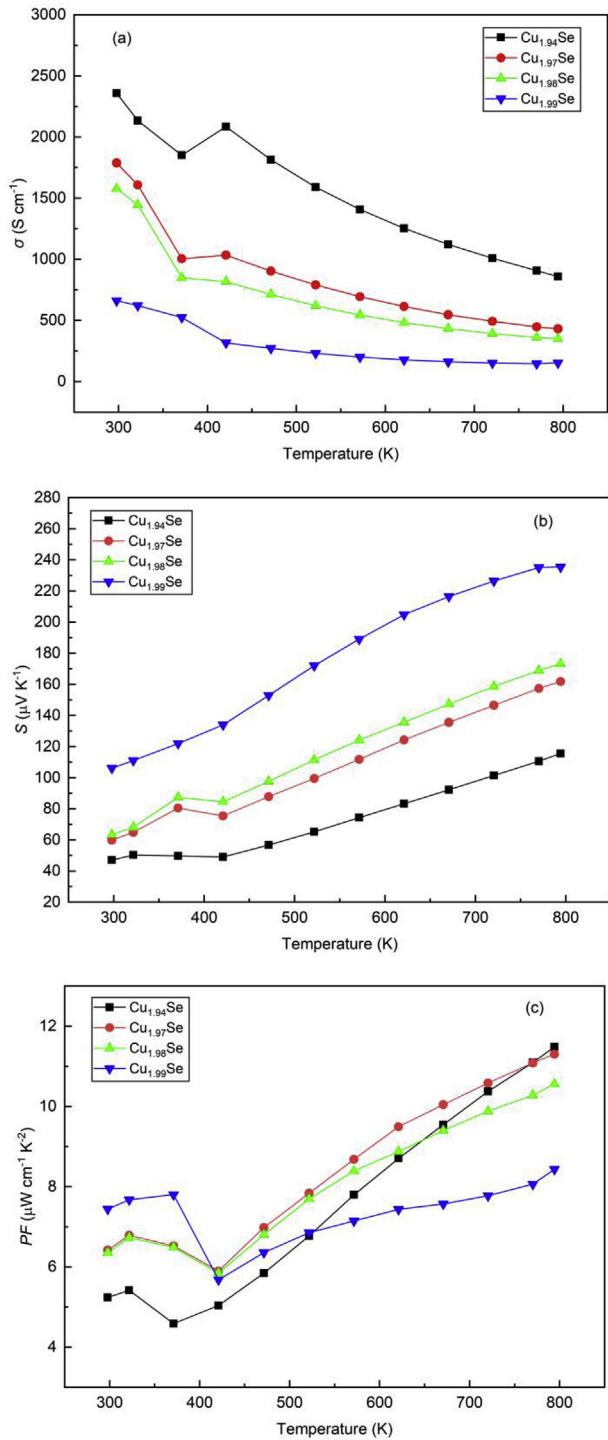


Fig. 3. Temperature dependence of electronic transport properties of Cu_{2-x}Se . (a) Electrical conductivity (b) Seebeck coefficient, and (c) Power factor.

adopted metallic limit Lorenz number derived from quantum mechanical treatment [54,55], which is represented by the dash line as shown in Fig. 6a. The metallic limit overestimates the electronic thermal conductivity, but underestimates the lattice thermal conductivity portion. Upon the calculated Lorenz number, the temperature-dependent electronic thermal conductivity κ_e is derived from the following equation and plotted in Fig. 6b,

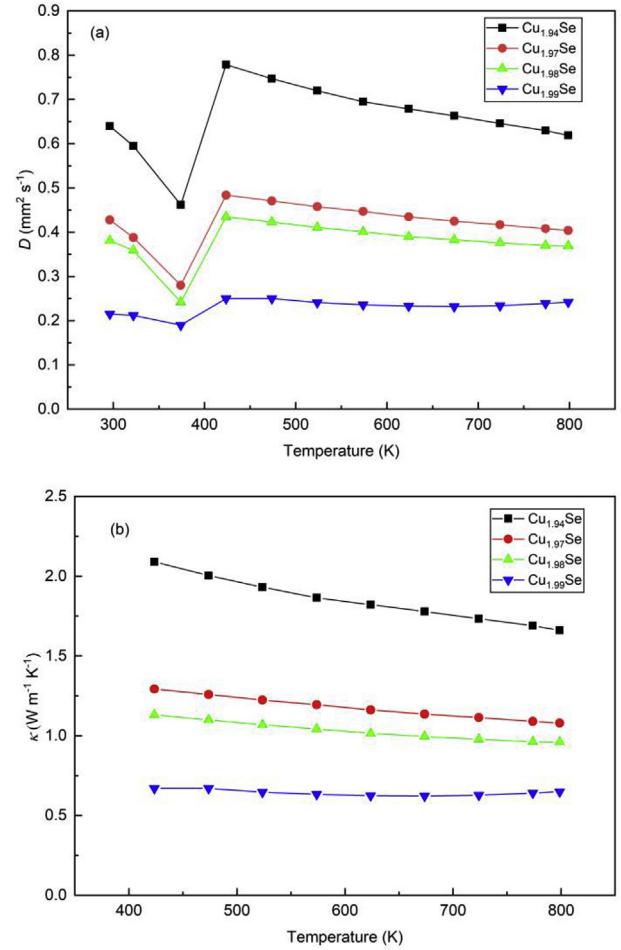


Fig. 4. Temperature dependence of thermal transport properties of Cu_{2-x}Se . (a) Thermal diffusivity of Cu_{2-x}Se and (b) Total thermal conductivity of β -phase Cu_{2-x}Se .

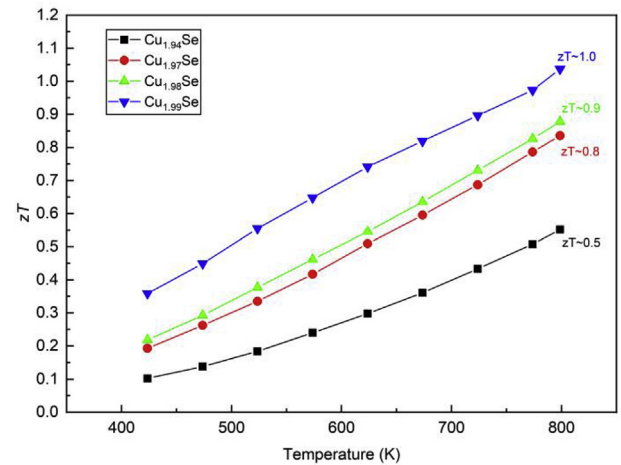


Fig. 5. Temperature dependence of TE figure of merit zT of β -phase Cu_{2-x}Se .

$$\kappa_e = L\sigma T \tag{3}$$

where σ is the electrical conductivity and T is the absolute temperature. In good agreement with the electrical conductivity analysis (Fig. 3a), the electronic thermal conductivity decreases with

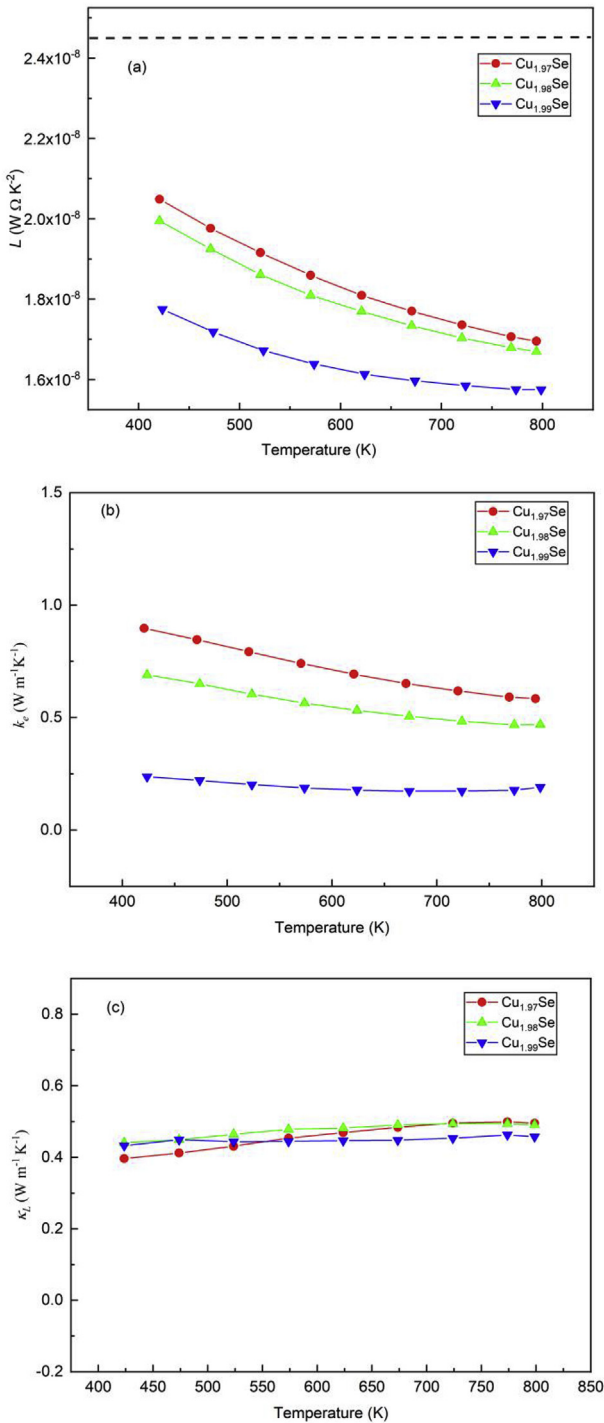


Fig. 6. Temperature dependence of calculated (a) Lorenz number, (b) Electronic thermal conductivity, and (c) Lattice thermal conductivity of β -phase Cu_{2-x}Se .

reducing Cu vacancies, indicating the strong response of electronic phonon transport to the carrier concentration in β -phase Cu_{2-x}Se . The electronic thermal conductivity also shows decrement against the increasing temperature, to explain this phenomenon, the enhanced phonon-carrier interaction as well as the superionic effect induced phonon-cation-diffusion interaction should be considered. With the experimental total thermal conductivity data and the calculated electronic thermal conductivity, the lattice thermal conductivity κ_L can be determined from the relationship:

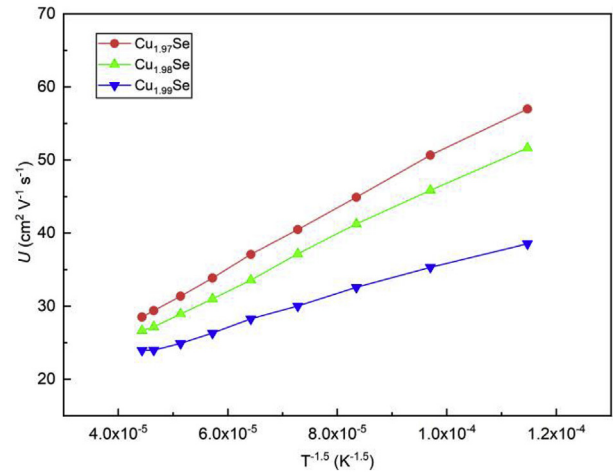


Fig. 7. Weighted mobility U of β -phase Cu_{2-x}Se , determined from the electrical conductivity and Seebeck coefficient data, as a function of exponential temperature ($T^{-1.5}$).

$\kappa_L = \kappa - \kappa_e$, as shown in Fig. 6c. For β -phase Cu_{2-x}Se , low lattice thermal conductivity of smaller than $0.5 \text{ W m}^{-1} \text{ K}^{-1}$ is obtained. In general, the lattice thermal conductivity is strongly temperature-dependent. However, the weak temperature dependence of lattice thermal conductivity is revealed for the samples, suggesting the suppressed lattice-vibration induced phonon transport by the liquid-like superionic behavior [56,57].

The electronic transport properties can be evaluated by determining the weighted mobility U for the $\text{Cu}_{1.97}\text{Se}$, $\text{Cu}_{1.98}\text{Se}$ and $\text{Cu}_{1.99}\text{Se}$ samples. For materials like superionic Cu_{2-x}Se , since the carrier mobility is too low to be precisely measured, Hall measurements are difficult to be effectively conducted at high temperature to obtain the effective mass m^* and the mobility parameter μ_0 , which determine the weighted mobility. Alternatively, the weighted mobility can be derived directly from the electrical conductivity and Seebeck coefficient, according to the equations [47],

$$\sigma = \sigma_{E_0} \cdot \ln(1 + e^{\eta}) \quad (4)$$

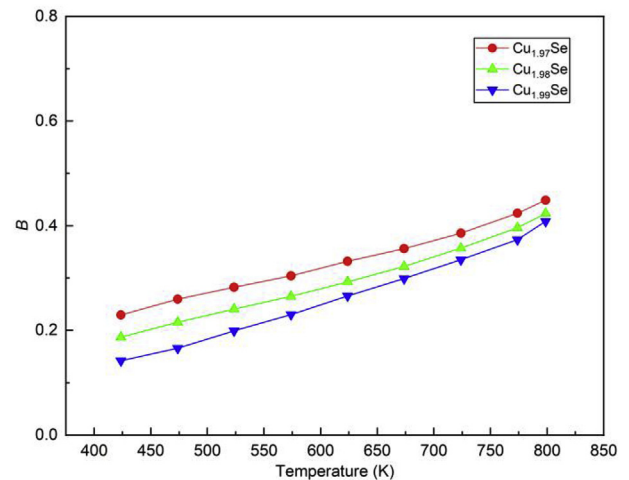


Fig. 8. Temperature dependence of quality factor B of β -phase Cu_{2-x}Se , derived from the electrical conductivity, Seebeck coefficient and lattice thermal conductivity data.

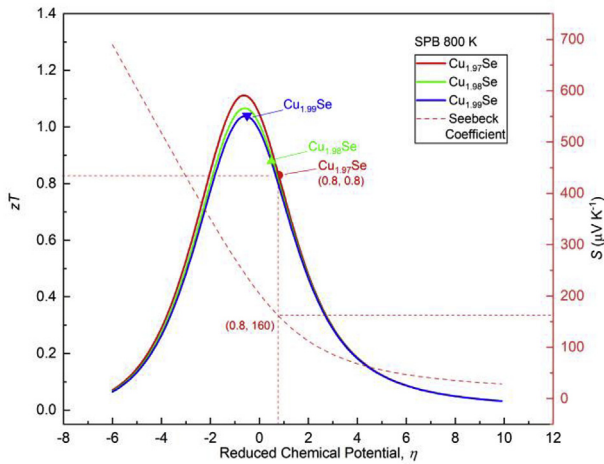


Fig. 9. Thermoelectric zT predicted by effective mass model (colored solid-curves) for Cu_{2-x}Se at 800 K and Seebeck coefficient (red dash-curve) as a function of reduced chemical potential, with the coordinate-located experimental zT values (represented by colored geometric dots).

$$U = \sigma_{E_0} \cdot \frac{3h^3}{8\pi e(2m_e k_B T)^{3/2}} \quad (5)$$

where σ_{E_0} is the transport coefficient, h is the Planck constant and

m_e is the electron mass. As presented in Fig. 7, the weighted mobility of all samples responds linearly to $T^{-1.5}$, indicating the charge transport is dominantly scattered by acoustic phonons. The continuous linearity of the curves also suggests that no bipolar effect takes place up to 800 K, and the cold-finger effect that would cause an abnormal increase of the weighted mobility at high temperature can be excluded for the Netzsch measurement system, as claimed by the system design.

With the electronic transport coefficient σ_{E_0} and the lattice thermal conductivity κ_L , the overall TE quality factor B , can be assessed from the following equation [58]:

$$B = \left(\frac{k_B}{e}\right)^2 \frac{\sigma_{E_0}}{\kappa_L} T. \quad (6)$$

As plotted in Fig. 8, the temperature-dependent quality factor is calculated for β -phase $\text{Cu}_{1.97}\text{Se}$, $\text{Cu}_{1.98}\text{Se}$ and $\text{Cu}_{1.99}\text{Se}$. Generally, the quality factor increases with more Cu vacancies and higher temperature, reaching >0.4 at 800 K for all samples, which indicates that the optimal zT of >1 should be achieved for as-fabricated Cu_{2-x}Se at this temperature.

After determining the quality factor, the zT can be predicted based on the relation:

$$zT = \frac{S^2}{L + \frac{(k_B/e)^2}{B \cdot \ln(1+e^\eta)}} \quad (7)$$

Fig. 9 exhibits the predicted zT (colored solid-curves) along with

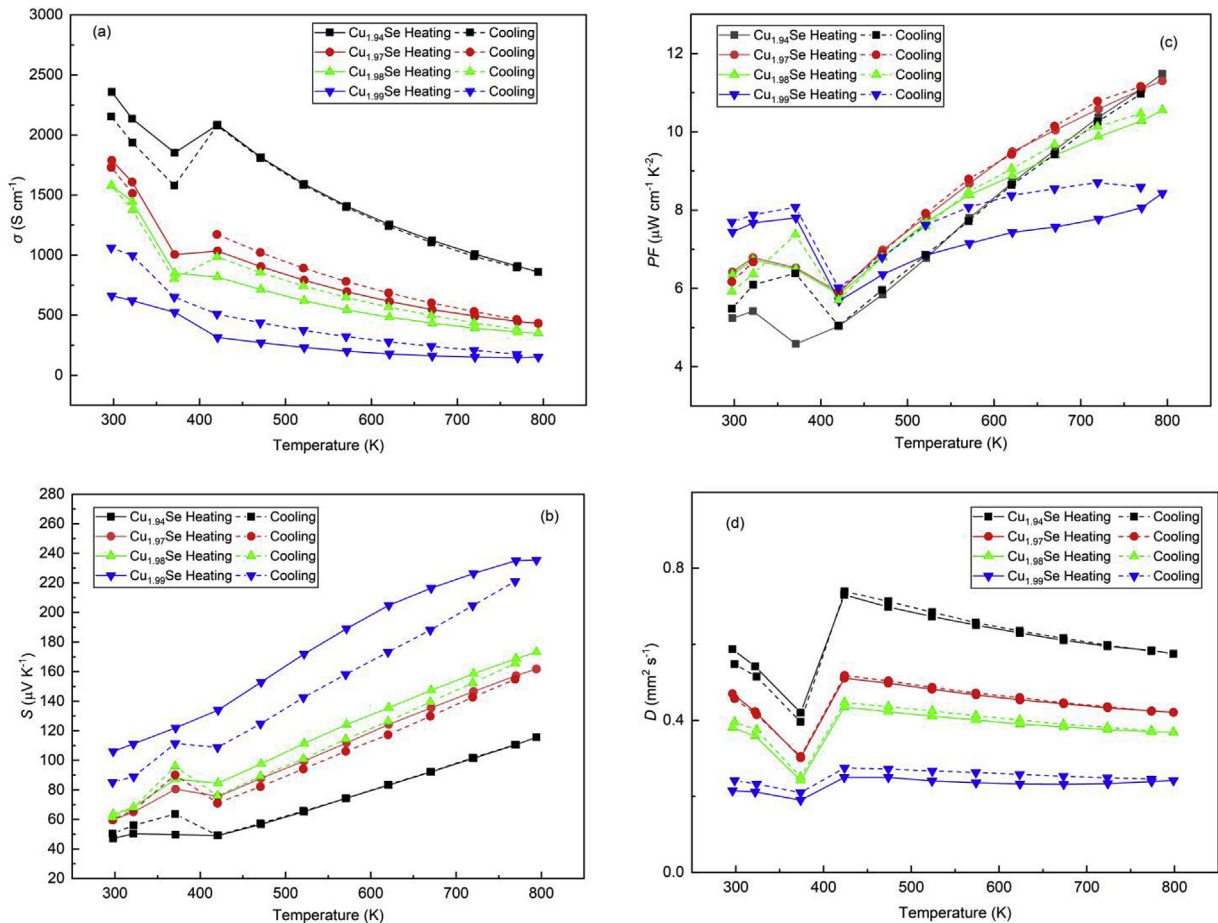


Fig. 10. Heating-cooling cycle test evaluations performed for Cu_{2-x}Se on electronic transport and thermal transport measurements. (a) Electrical conductivity (b) Seebeck coefficient (c) Calculated cycling power factor derived from the electrical conductivity and Seebeck coefficient ($PF = S^2\sigma$) (d) Thermal diffusivity.

the Seebeck coefficient (red dash-curve) as a function of reduced chemical potential η for $\text{Cu}_{1.97}\text{Se}$, $\text{Cu}_{1.98}\text{Se}$ and $\text{Cu}_{1.99}\text{Se}$ at 800 K. It is found that the experimental zT values (represented by colored geometric dots) match well with the predictions for all samples. Taking $\text{Cu}_{1.97}\text{Se}$ as an instance, the measured zT and Seebeck coefficient at 800 K are 0.8 and $162 \mu\text{V K}^{-1}$ respectively, making a very good agreement with the prediction (0.8 for zT and $160 \mu\text{V K}^{-1}$ for Seebeck coefficient). As a result, based on the precise model prediction and Cu-vacancy engineering, the zT is optimized to the maximum value of 1.0 in $\text{Cu}_{1.99}\text{Se}$ that is comparable to that of undoped Cu_{2-x}Se when compared with other reported works [47,48].

To investigate the repeatability in properties of the as-fabricated Cu_{2-x}Se samples, heating-cooling cycle tests are conducted for the electrical conductivity, Seebeck coefficient and thermal diffusivity measurements. Along with the calculated cycling power factors, the results are presented in Fig. 10. All the measurements show good repeatability upon the heating-cooling process over the whole temperature range up to 800 K, regardless of the hysteresis behavior exhibited during the phase-transition region. The good repeatability achieved is amongst the best ones that reported for the Cu_{2-x}Se -based TE materials [46–48,59]. Besides, changes are observed among the repeatability in properties of the Cu_{2-x}Se samples. The changes can be explained by small changes in Cu vacancy content during the measurement. As the samples are heated the Seebeck is higher and electrical conductivity are lower than they are for cooling. This suggests that at high temperature more copper vacancies form that also increases the hole concentration. Thus on cooling there are more charge carriers that decrease the Seebeck, increase the electrical conductivity and also alter the electronic contribution to the thermal conductivity. At lower temperature the copper could very well be reabsorbed. For a given change in copper vacancies, samples already with more copper vacancies have a smaller relative change and therefore their properties are less sensitive to thermal variations.

4. Conclusions

In conclusion, with the scalable fabrication technology, the optimized Cu_{2-x}Se exhibits good TE properties with the optimal zT of ~ 1.0 at 800 K. The optimization is carried out based on the precise Cu-vacancy engineering using effective mass modeling as a guide. The good TE performance is contributed from the as-obtained high power factor and low thermal conductivity, for which, the mechanism analyses including electronic transport and thermal transport properties are discussed. Both the electronic transport and the thermal transport are highly dependent on the Cu-vacancy concentration. Meanwhile, we explore the changes in properties upon heating and cooling for the Cu_{2-x}Se samples. Our study provides a promising and realizable approach of using Cu-vacancy engineering and modeling to advance the TE performance as well as promote the potential of practical application for Cu_{2-x}Se .

Conflicts of interest

Authors declare that there are no conflicts of interest.

Funding

This work was funded by The Hong Kong Polytechnic University [grant numbers 1-ZVGH, DD7F].

References

[1] Bell LE. Cooling, heating, generating power, and recovering waste heat with thermoelectric systems. *Science* 2008;321:1457–61.

- [2] Disalvo FJ. Thermoelectric cooling and power generation. *Science* 1999;285:703–6.
- [3] Hochbaum AI, et al. Enhanced thermoelectric performance of rough silicon nanowires. *Nature* 2008;451:163–7.
- [4] Kanatzidis MG. Nanostructured thermoelectrics: the new paradigm? *Chem Mater* 2010;22:648–59.
- [5] Zhang X, Zhao LD. Thermoelectric materials: energy conversion between heat and electricity. *J Materiomics* 2015;1:92–105.
- [6] Snyder GJ, Toberer ES. Complex thermoelectric materials. *Nat Mater* 2008;7:105–14.
- [7] Tan G, Zhao LD, Kanatzidis MG. Rationally designing high-performance bulk thermoelectric materials. *Chem Rev* 2016;116:12123–49.
- [8] He J, Tritt TM. Advances in thermoelectric materials research: looking back and moving forward. *Science* 2017;357:9997.
- [9] Li JF, Pan Y, Wu CF, et al. Processing of advanced thermoelectric materials. *Sci China Technol Sci* 2017;60:1347–64.
- [10] Pan Y, Aydemir U, Grovogui JA, et al. Melt-centrifuged (Bi, Sb)₂Te₃: engineering microstructure toward high thermoelectric efficiency. *Adv Mater* 2018;30:1802016.
- [11] Li JF, Liu WS, Zhao LD, et al. High-performance nanostructured thermoelectric materials. *NPG Asia Mater* 2010;2:152–8.
- [12] Yang JH, Caillat T. Thermoelectric materials for space and automotive power generation. *MRS Bull* 2006;31:224–9.
- [13] Nunna R, Qiu PF, Yin M, et al. Ultrahigh thermoelectric performance in Cu₂Se-based hybrid materials with highly dispersed molecular CNTs. *Energy Environ Sci* 2017;10:1928–35.
- [14] Sales BC. Thermoelectric materials. Smaller is cooler. *Science* 2002;295:1248–9.
- [15] Nolas GS, Poon J, Kanatzidis M. Recent developments in bulk thermoelectric materials. *MRS Bull* 2006;31:199–205.
- [16] Yang L, Chen ZG, Dargusch MS, Zou J. High performance thermoelectric materials: progress and their applications. *Adv Energy Mater* 2017;8:1701797.
- [17] Sootsman JR, Chung DY, Kanatzidis MG. New and old concepts in thermoelectric materials. *Angew Chem Int Ed Engl* 2009;48:8616–39.
- [18] Mori T. Novel principles and nanostructuring methods for enhanced thermoelectrics. *Small* 2017;13:1702013.
- [19] Szczech JR, Higgins JM, Jin S. Enhancement of the thermoelectric properties in nanoscale and nanostructured materials. *J Mater Chem* 2011;21:4037–55.
- [20] Christensen M, Abrahamsen AB, Christensen NB, et al. Avoided crossing of rattler modes in thermoelectric materials. *Nat Mater* 2008;7:811–5.
- [21] Heremans JP, Jovovic V, Toberer ES, Saramat A, Kurosaki K, Charoenphakdee A, et al. Enhancement of thermoelectric efficiency in PbTe by distortion of the electronic density of states. *Science* 2008;321:554–7.
- [22] Zhang Q, Wang H, Liu W, Wang H, Yu B, et al. Enhancement of thermoelectric figure-of-merit by resonant states of aluminium doping in lead selenide. *Energy Environ Sci* 2012;5:5246–51.
- [23] Hong M, Chen ZG, Yang L, Zou YC, Dargusch MS, Wang H, et al. Realizing zT of 2.3 in $\text{Ge}_{1-x}\text{Sb}_x\text{In}_y\text{Te}$ via reducing the phase-transition temperature and introducing resonant energy doping. *Adv Mater* 2018;30:1705942.
- [24] Hong M, Chen ZG, Yang L, Liao ZM, Zou YC, Chen YH, et al. Achieving $zT > 2$ in p-Type $\text{AgSbTe}_{2-x}\text{Se}_x$ alloys via exploring the extra light valence band and introducing dense stacking faults. *Adv Energy Mater* 2018;8:1702333.
- [25] Burke PG, Curtin BM, Bowers JE, Gossard AC. Minority carrier barrier heterojunctions for improved thermoelectric efficiency. *Nano Energy* 2015;12:735–41.
- [26] Liu X, Zhu T, Wang H, Hu L, Xie H, Jiang G, et al. Low electron scattering potentials in high performance $\text{Mg}_2\text{Si}_{0.45}\text{Sn}_{0.55}$ based thermoelectric solid solutions with band convergence. *Adv Energy Mater* 2013;3:1238–44.
- [27] Tian Y, Sakr MR, Kinder JM, Liang D, MacDonald MJ, Qiu RL, et al. One dimensional quantum confinement effect modulated thermoelectric properties in InAs nanowires. *Nano Lett* 2012;12:6492–7.
- [28] Hong M, Chasapis TC, Chen ZG, Yang L, Kanatzidis MG, Snyder GJ, et al. n-Type $\text{Bi}_2\text{Te}_{3-x}\text{Se}_x$ nanoplates with enhanced thermoelectric efficiency driven by wide-frequency phonon scatterings and synergistic carrier scatterings. *ACS Nano* 2016;10:4719–27.
- [29] Yang L, Chen ZG, Hong M, Han G, Zou J. Enhanced thermoelectric performance of nanostructured Bi_2Te_3 through significant phonon scattering. *ACS Appl Mater Interf* 2015;7:23694–9.
- [30] Bhattacharya S, Bohra A, Basu R, Bhatt R, Ahmad S, Meshram K, et al. High thermoelectric performance of $(\text{AgCrSe}_2)_{0.5}(\text{CuCrSe}_2)_{0.5}$ nano-composites having all-scale natural hierarchical architectures. *J Mater Chem A* 2014;2:17122–9.
- [31] Poudel B, Hao Q, Ma Y, Lan Y, Minnich A, Yu B, et al. High-thermoelectric performance of nanostructured bismuth antimony telluride bulk alloys. *Science* 2008;320:634–8.
- [32] Biswas K, He J, Blum ID, Wu CI, Hogan TP, Seidman DN, et al. High performance bulk thermoelectrics with all-scale hierarchical architectures. *Nature* 2012;489:414–8.
- [33] Moshwan R, Yang L, Zou J, Chen ZG. Eco-friendly SnTe thermoelectric materials: progress and future challenge. *Adv Funct Mater* 2017;27:1703278.
- [34] Han G, Chen ZG, Drennan J, Zou J. Indium selenides: structural characteristics, synthesis and their thermoelectric performances. *Small* 2014;10:2747–65.
- [35] Chen X, Girard SN, Meng F, Lara-Curzio E, Jin S, Goodenough JB, Zhou J, Shi L. Approaching the minimum thermal conductivity in rhenium-substituted high manganese silicides. *Adv Energy Mater* 2014;4:1–10.

- [36] Slack GA. In: Rowe DM, editor. CRC handbook of thermoelectrics. CRC Press; 1995. p. 407–40.
- [37] Voneshen D, Walker HC, Refson K, Goff JP. Hopping time scales and the phonon-liquid electron-crystal picture in thermoelectric copper selenide. *Phys Rev Lett* 2017;118:145901.
- [38] Brown DR, Heijl R, Borup KA, et al. Relating phase transition heat capacity to thermal conductivity and effusivity in Cu_2Se . *Phys Status Solidi RRL* 2016;10: 618–21.
- [39] Vasilevskiy D, Keshavarz MK, Simard JM, et al. Assessing the thermal conductivity of Cu_{2-x}Se alloys undergoing a phase transition via the simultaneous measurement of thermoelectric parameters by a Harman-based setup. *J Electron Mater* 2018;47:3314–9.
- [40] Kang SD, Danilkin SA, Aydemir U, et al. Apparent critical phenomena in the superionic phase transition of Cu_{2-x}Se . *New J Phys* 2016;18:013024.
- [41] Brown DR, Day T, Borup KA, et al. Phase transition enhanced thermoelectric figure-of-merit in copper chalcogenides. *APL Mater* 2013;1:052107.
- [42] Horvatic M, Vucic Z. Dc ionic conductivity measurements on the mixed conductor Cu_{2-x}Se . *Solid State Ionics* 1984;13:117–25.
- [43] Gulay L, Daszkiewicz M, Strok O, Pietraszko A. Crystal structure of Cu_2Se . *Chem Met Alloys* 2011;4:200–5.
- [44] Heyding RD, Murray RM. The crystal structures of $\text{Cu}_{1.8}\text{Se}$, Cu_3Se_2 , α - and γ CuSe , CuSe_2 , and CuSe_2II . *Can J Chem* 1976;54:841–8.
- [45] Oliveria M, McMullan RK, Wuensch BJ. Single crystal neutron diffraction analysis of the cation distribution in the high-temperature phases α - Cu_{2-x}S , α - Cu_{2-x}Se , and α - Ag_2Se . *Solid State Ionics* 1988;28:1332–7.
- [46] Olvera AA, Moroz NA, Sahoo P, Ren P, Bailey TP, Page AA, Uher C, Poudeu PFP. Partial indium solubility induces chemical stability and colossal thermoelectric figure of merit in Cu_2Se . *Energy Environ Sci* 2017;10:1668–76.
- [47] Kang SD, Pöhls JH, Aydemir U, et al. Enhanced stability and thermoelectric figure-of-merit in copper selenide by lithium doping. *Mater Today Phys* 2017;1:7–13.
- [48] Qiu P, Agne MT, Liu Y, et al. Suppression of atom motion and metal deposition in mixed ionic electronic conductors. *Nat Commun* 2018;9:2910.
- [49] Zevalkink A, Zeier WG, Cheng E, et al. Nonstoichiometry in the zintl phase $\text{Yb}_{1-\delta}\text{Zn}_2\text{Sb}_2$ as a route to thermoelectric optimization. *Chem Mater* 2014;26: 5710–7.
- [50] Zevalkink A, Smiadak DM, Blackburn JL, et al. A practical field guide to thermoelectrics: fundamentals, synthesis, and characterization. *Appl Phys Rev* 2018;5:021303.
- [51] Liu H, Shi X, Xu FF, et al. Copper ion liquid-like thermoelectrics. *Nat Mater* 2012;11:422–5.
- [52] Shen J, Chen Z, Lin S, Zheng L, Li W, Pei Y. Single parabolic band behavior of thermoelectric p-type CuGaTe_2 . *J Mater Chem C* 2016;4:209–14.
- [53] Liu WD, Shi XL, Moshwan R, et al. Enhancing thermoelectric performance of $(\text{Cu}_{1-x}\text{Ag}_x)_2\text{Se}$ via CuAgSe secondary phase and porous design. *Sustain Mater Technol* 2018;17:e00076.
- [54] Toberer ES, Cox CA, Brown SR, et al. Traversing the metal-insulator transition in a zintl phase: rational enhancement of thermoelectric efficiency in $\text{Yb}_{14}\text{Mn}_{1-x}\text{Al}_x\text{Sb}_{11}$. *Adv Funct Mater* 2008;18:2795–800.
- [55] Kumar GS, Prasad G, Pohl RO. Experimental determinations of the Lorenz number. *J Mater Sci* 1993;28:4261–72.
- [56] Slack GA. The thermal conductivity of nonmetallic crystals. *Solid State Phys* 1979;34:1–71.
- [57] Kazem N, Zaikina JV, Ohno S, et al. Coinage-metal-stuffed $\text{Eu}_9\text{Cd}_4\text{Sb}_9$: metallic compounds with anomalous low thermal conductivities. *Chem Mater* 2015;27:7508–19.
- [58] Kang SD, Snyder GJ. Charge-transport model for conducting polymers (Supplementary Information). *Nat Mater* 2017;16:252–7.
- [59] Md S, Islam KN, Li M, et al. Giant enhancement of the figure-of-merit over a broad temperature range in nano-boron incorporated Cu_2Se . *J Mater Chem A* 2018;6:18409–16.



Zhiming Geng received the M.Phil. degree in School of Materials Science and Engineering from Changzhou University in 2015. During his studies, he worked on processing and characterization of photoelectric and piezoelectric materials and their applications. In addition, he has also advanced the national project on research & development of advanced package and test technology for sensor chips. His recent research direction includes thermoelectric materials and functional device technologies.



Dongliang Shi is now a Ph.D. candidate in the Hong Kong Polytechnic University. He received the M.Phil. degree in School of Materials Science and Engineering from the Changzhou University in 2013. During his graduate studies, he worked on processing and characterization of piezoelectric materials and their sensing applications. He has also been working in the field of smart multifunctional materials, such as magnetoelectric materials, and their applications. His recent research interests include thermoelectric materials, and their sensing and energy harvesting applications.



Lu Shi is a postdoctoral researcher in the Hong Kong Polytechnic University. She received the Ph.D. degree from Beijing Institute of Technology (BIT) in 2016. Her current research interests focus on the development of advanced nanostructured electrode materials for energy storage applications, including lithium-ion batteries, lithium-sulfur batteries, sodium-ion batteries and potassium-ion batteries.



Ying Li is now a Ph.D. candidate in the Hong Kong Polytechnic University. She received the B.Sc. degree of Chemical Education and the M.Sc. degree majored in Materials Science in College of Chemistry and Materials Science from Sichuan Normal University in 2012 and 2015, respectively. During her graduate studies, she engaged in the research and development of BFO-based multiferroic ceramics. She has also been working in the field of lithium-ion battery cathode materials. Her recent research interests include Li/Na-ion battery cathode materials and electrocatalysts.



G. Jeffrey Snyder is a Professor of Materials Science and Engineering at Northwestern University in Evanston Illinois. His research interests focus on materials physics and chemistry for thermoelectric engineering such as band engineering, design of complex Zintl compounds and use of nanostructured composites. His interdisciplinary approach stems from studies of Solid State Chemistry at Cornell University and the Max Planck Institute for solid state research, Applied Physics at Stanford University, and thermoelectric materials & device engineering at NASA/Jet Propulsion Laboratory and California Institute of Technology (Caltech).



Kwok-ho Lam received his Ph.D. degree in Applied Physics from The Hong Kong Polytechnic University (HKPolyU). Before became a faculty member in HKPolyU, he was a Research Associate at the National Institutes of Health Resource Center on Medical Ultrasonic Transducer Technology in Department of Biomedical Engineering of the University of Southern California. He is currently an Associate Professor in Department of Electrical Engineering at HKPolyU. His research interests focus on energy materials including piezoelectric, dielectric, thermoelectric materials, and electrode materials for rechargeable batteries, and ultrasound transducer technology for biomedical and non-destructive evaluation applications.